Novel Zero-Sequence Current Excited Double-Sided Vernier Reluctance Linear Machine with High-Order -Harmonic Toroidal Winding

Zhenghao Li, Feifan Ni, Shuangxia Niu and Kwok Tong Chau

Department of Electrical and Electronic Engineering, Hong Kong Polytechnic University, Hong Kong, China

Abstract — Double-sided Vernier reluctance linear machine (DS-VRLM) is very suitable for long stroke applications, taking advantages of magnet-free design, eliminated magnetic pull and high thrust force density. Aiming to eliminate extra DC coils in DS-VRLM, and further boost the thrust force density of it, a novel non-overlapped double-layer integrated toroidal winding design excited by zero-sequence current is proposed in this paper. The key to achieving this is to utilize artificial arrangement of integrated toroidal winding to generate spatial high-order harmonic of magnetic field for higher pole pair number and gear ratio to acquire enhanced thrust density. Meanwhile, thanks to the toroidal winding configuration, the integrated toroidal winding could make full use of working harmonics, contributing to enhanced winding factor.

***Index Terms*—Vernier reluctance linear machine, zero-sequence current, flux modulation**

I. Introduction

Linear motors are widely used in the fields of transportation and industrial automation due to their advantages of simple structure, high precision and simple maintenance [1]-[2]. Considering the fluctuating prices of permanent magnet (PM), and its potential demagnetization problem, the PM-free linear machines have been attracting much research attention. Among the various types of PM-free linear machines, linear synchronous reluctance motors (LSRMs) stand out due to their simplicity and robustness [3]. LSRMs are designed to operate efficiently without the need for permanent magnets, making them a cost-effective and reliable choice for many applications. Although these motors have simple control methods, their efficiency and force density are too low for some industrial applications. Other PM-free linear machines include the linear switched reluctance machines (LSRMs) [4] and the linear variable reluctance machines (LVFRMs) [5]-[6]. LSRMs operate based on the principle of reluctance, utilizing a simple and robust design that relies on the magnetic attraction between the mover and stator to produce linear motion. Four different LSRMs topologies are compared in [7] and the result shows that two of them are infeasible for vertical elevator applications as their force density is too low. The model with the highest force density also has the largest copper winding loss. LVFRMs are doubly excited by armature winding and DC field winding. Thus, the air-gap flux can be controlled to extend the power range. However, high thrust force ripples and low power factor still exist [8]. In order to reduce the force ripple while maintaining the force density, multi-tooth LVFRM is proposed in [9]. It is shown that four-tooth LVFRM can provide lower force ripple than that of single-tooth LVFRM at relatively low copper loss. Nonetheless, since the multi-tooth structure still does not address the poor excitation issue of LVFRMs, their thrust force density remains low.

To address the challenge of low thrust force density in PM-free linear machines, the Vernier reluctance linear machine (VRLM) has been proposed, as detailed in [10]. This innovative design leverages the flux modulation effect of DC excitations to enhance performance. By effectively utilizing both fundamental and high-order harmonics generated by the DC field winding, the winding factor of the armature winding is significantly improved. This approach not only optimizes the electromagnetic interaction but also enhances the overall efficiency and thrust capability of the machine, making it a promising solution for applications requiring high thrust density without the use of PMs.

In this paper, to eliminate DC winding and boost the thrust force of VRLM, a novel double layer integrated toroidal winding design (DL-ITW) excited by zero-sequence current is proposed for double-sided Vernier reluctance linear machine (DS-VRLM), which retains the benefits of a robust structure and controllable excitation field found in the existing Vernier reluctance machines (VRMs) [11]-[12]. By integrating the winding design, the system achieves improved performance without the complexity and additional components associated with separate DC windings. This advancement not only simplifies the machine structures but also enhances its thrust force density. The main working harmonics of the proposed machine is modulated from third-order harmonic of excited magnetic field to enhance the DS-VRLMs' force density. The rest of this article is organized as follows. In Section II, the machine structure of the proposed DS-VRLM and working principle are introduced with the analysis of the air-gap harmonic. The feasibility of the novel high-order winding is also verified. In Section III, the dimension of the proposed model is listed and the electromagnetic performances of different slot-pole combinations are analyzed and compared. Finally, the conclusion is drawn in Section V.

II. Machine Structure and Operation Principle

A. Machine structure

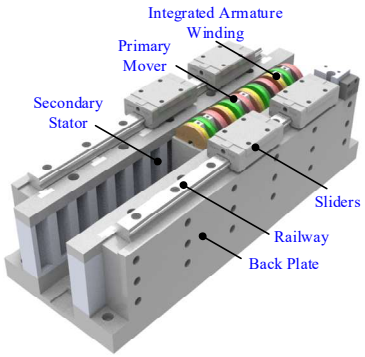

Fig. 1. Machine structure of the proposed DS-VRLM

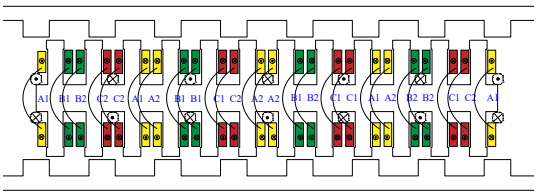

Fig. 2. Winding configuration of the proposed DS-VRLM

The machine structure is shown in Fig.1. The primary mover features a double-sided design with 12 slots on each side. There are double layers of windings in each mover slot. The secondary stators use salient-pole teeth to form a doubly salient structure, symmetrically positioned on either side of the mover. The Fig.2 shows the winding configuration of newly proposed DS-VRLM, whose armature winding adopts a double-layer toroidal winding connection. To be noticed, two coils in the same phase are arranged in the same slot but divided into winding 1 and winding 2, which have opposite polarity of zero-sequence current. The direction of the equivalent DC current for the zero-sequence current is also indicated in Fig.2. Taking Phase A as an example, equivalent field current exists in the slot only housing winding A1 or A2 when zero-sequence current exists, whose direction is consistent with winding A1 or A2, and no equivalent field current exists for the slot housing both winding A1 and A2. All coils in the same winding set, e.g. A1 or A2, are connected in series. The magnitude of the zero-sequence current can be adjusted, allowing for flexible regulation of the excitation field. This provides advantages for flux weakening and fast fault demagnetization.

B. Control method and working principle

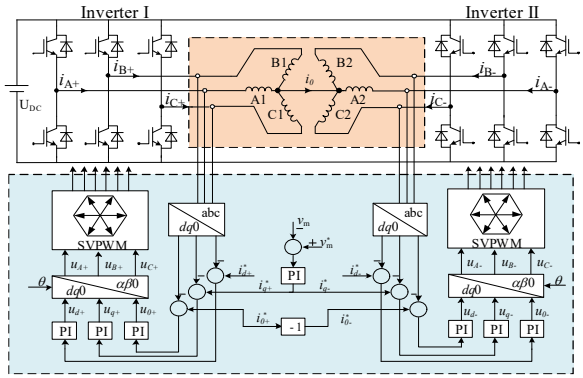

Fig. 3. Control scheme of the proposed DS-VRLM

In contrast to the vector control typically employed in traditional machines, Fig. 3 presents the speed control scheme specifically designed for the proposed DS-VRLM excited by zero-sequence current. The motor retains a three-phase design; however, the windings in each phase are divided into two groups. For instance, phase A comprises two winding groups, labeled A1 and A2. The detailed expressions for the current in each winding are formulated as follows

$$\begin{cases} i_{\mathrm{A1}}(t) = I_{\max}\sin(\omega_{\mathrm{e}}\, t + \theta_{\mathrm{e}}) + I_{\mathrm{dc}} \\ i_{\mathrm{A2}}(t) = I_{\max}\sin(\omega_{\mathrm{e}}\, t + \theta_{\mathrm{e}}) - I_{\mathrm{dc}} \\ i_{\mathrm{B1}}(t) = I_{\max}\sin\left(\omega_{\mathrm{e}}\, t + \theta_{\mathrm{e}} - \frac{2\pi}{3}\right) + I_{\mathrm{dc}} \\ i_{\mathrm{B2}}(t) = I_{\max}\sin\left(\omega_{\mathrm{e}}\, t + \theta_{\mathrm{e}} - \frac{2\pi}{3}\right) - I_{\mathrm{dc}} \\ i_{\mathrm{C1}}(t) = I_{\max}\sin\left(\omega_{\mathrm{e}}\, t + \theta_{\mathrm{e}} + \frac{2\pi}{3}\right) + I_{\mathrm{dc}} \\ i_{\mathrm{C2}}(t) = I_{\max}\sin\left(\omega_{\mathrm{e}}\, t + \theta_{\mathrm{e}} + \frac{2\pi}{3}\right) - I_{\mathrm{dc}} \end{cases} \quad (1)$$

where θ_{e} is the initial electrical angle and ω_{e} is the electrical angular speed of the motor's move which has the following relationship with the mover's mechanical angle.

$$\omega_{\mathrm{e}} = N_r \frac{d\theta_r}{dt} \quad (2)$$

As shown in Fig.3, two inverters will be used to control the current: i_{A1}, i_{B1}, and i_{C1} are supplied by Inverter I, while i_{A2}, i_{B2}, and i_{C2} are supplied by Inverter II. Each current is the combination of the AC current component $I_{\max}$ and the DC current component I_{dc}. I_{dc} is proportional to i_0. Specifically, the zero-sequence current from inverter I can be written as

$$i_{0+} = \sqrt{3} i_{dc} \quad (3)$$

The zero-sequence current from inverter II can be written as

$$i_{0-} = -\sqrt{3} i_{dc} \quad (4)$$

Their relationship can be derived using the Clarke and Park transformer matrix.

$$\begin{bmatrix} i_d \\ i_q \\ i_0 \end{bmatrix} = \begin{bmatrix} \cos\theta_r & -\sin\theta_r & 0 \\ \sin\theta_r & \cos\theta_r & 0 \\ 0 & 0 & 1 \end{bmatrix} \cdot \sqrt{\frac{2}{3}} \begin{bmatrix} 1 & -\frac{1}{2} & -\frac{1}{2} \\ 0 & \frac{\sqrt{3}}{2} & -\frac{\sqrt{3}}{2} \\ \frac{\sqrt{2}}{2} & \frac{\sqrt{2}}{2} & \frac{\sqrt{2}}{2} \end{bmatrix} \begin{bmatrix} i_A \\ i_B \\ i_C \end{bmatrix} \quad (5)$$

Hence, the equivalent DC current can be controlled effectively by controlling i_0.

C. High-Order-Harmonic winding design and working principle

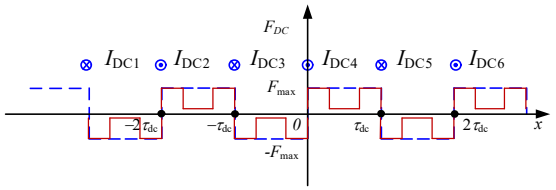

Fig. 4. MMF excited by DC current component.

According to the special arrangement of equivalent field current, which is distributed alternatively every two slots as shown in Fig.2, the magnetomotive force generated by the DC current component is shown in Fig.4. The blue line is the MMF before the modulation process which can be written as Eq.6. The red line represents the MMF after modulated by the mover teeth that can be calculated as Eq.7.

$$F_{dc}(x) = \sum_{j=1,3,5\ldots} \frac{4N_{turn}I_{dc}}{j\pi} \sin\left(\frac{j\pi}{\tau_{\mathrm{dc}}} x\right) \quad (6)$$

$$F'_{\mathrm{dc}}(x) = F_{\mathrm{dc}}(x) \cdot \Lambda_m(x) = \sum_{j=1,3,5\ldots} \sum_{n_1=0,1,2\ldots} \frac{2F_{max}}{j\pi} \cdot \frac{2\Lambda_{\mathrm{m}}}{n_1\pi} \sin\left(\frac{2n_1\pi}{\tau_{\mathrm{dc}}} x_1\right) \sin\left[\left(j \pm 4n_1\right)\frac{\pi}{\tau_{dc}}\, x\right] \quad (7)$$

where $F_{\max}$ is the maximum value of MMF of the equivalent DC excitation, j is the order of the MMF harmonics, x_1 is the width of the mover slot, and τ_{dc} is the distance between two adjacent equivalent DC field current coils, $\Lambda_{\mathrm{m}}(x)$ is the permeance of the mover teeth. Hence, the pole pair number of the MMF harmonic of the equivalent DC excitation of the zero-sequence current can be expressed as

$$P'_{zs} = kP_{zs} \quad (8)$$

$$k = j \pm 4n_1 \quad (9)$$

The air-gap flux density can be calculated by multiplying the MMF harmonic of the equivalent DC excitation and the permeance of salient stator.

$$B_{(j,n1,n2)}(x,t) = F'_{\mathrm{dc}}(x)\cdot\Lambda_s(x,t) = \sum_{n_2=0,1,2\ldots}\sum_{j=1,3,5\ldots}\sum_{n1=0,1,2\ldots}\frac{F_{max}}{j\pi}\cdot \frac{2\Lambda_{\mathrm{m}}}{n_1\pi}\sin\left(\frac{2n_1\pi}{\tau_{\mathrm{dc}}}x_1\right)\cdot\frac{2\Lambda_{\mathrm{s}}}{n_2\pi}\sin\left(\frac{n_2\pi}{\tau_{\mathrm{s}}}x_2\right)\cdot\sin\left\{\frac{2\pi}{L_{\mathrm{m1}}}\left[\left((j\pm 4n_1)P_{\mathrm{zs}}\pm n_2N_{\mathrm{s}}\right)\left(x+\frac{n_2N_{\mathrm{s}}}{(j\pm4n_1)P_{\mathrm{zs}}\pm n_2N_{\mathrm{s}}}v_{\mathrm{m}}t\right)\right]\right. \quad (10)$$

where τ_{s} is the pole pitch of the stator teeth, x_2 is the width of stator slot and N_{s} is the number of stator teeth. According to flux modulation theory, the proposed DS-VRLM are designed to utilize working harmonics whose pole pair number (PPN) is expressed as,

$$P_{\mathrm{w}} = |kP_{zs} \pm n_2N_{\mathrm{s}}| \quad (11)$$

When k and n take on different values, various armature winding designs can be achieved, each corresponding to different order of main working harmonics. Generally, $n_2 = 1$. In the case of a machine using conventional fundamental harmonics, the value of k is equal to 1. As there are higher-order harmonics of field current, especially third-order harmonic, which could be utilized to generate working harmonics and this means $k = 3$ in this case. Taking machine with 12/7 slot/pole combination as example, the gear ratio of the working harmonic can be improved from 1.75 to 3.5 compared with machine using conventional fundamental harmonic. Fig.5 is the detailed proposed winding connection. Due to the introduction of zero-sequence current, each phase winding is divided into two groups. These groups in the same phase share the same AC component, but the zero-sequence currents are in opposite directions.

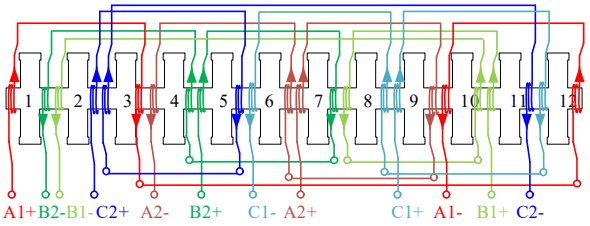

Fig. 5. Winding connection.

From the Eq.12, it can be seen that the mechanical speed of the working harmonics of the j-th order is

$$v_j = G_r v_m \quad (12)$$

where G_r is the gear ratio. The lower the order of the working harmonics, the higher the mechanical speed that can be achieved. Therefore, utilizing higher-order harmonics as working harmonics can contribute to enhanced induced voltage, as the open-circuit induced voltage of one phase can be calculated as follows.

$$e_j(t) = -\frac{d\psi_j(t)}{dt} = 2l_{\mathrm{stk}}B_{(j,n1,n2)}k_{\mathrm{wn}}G_r v_{\mathrm{m}}\sin\left(\frac{2\pi}{L_x}n_2N_s v_m t\right) \quad (13)$$

The winding factor can be calculated as follows and the comparison result of different windings is shown in the table. τ_{w} is the pole pitch of working harmonic.

$$\begin{cases} k_{\mathrm{wn}} = k_{\mathrm{pn}}k_{\mathrm{dn}} \\ k_{\mathrm{pn}} = \sin\frac{\tau_{\mathrm{ac}}}{\tau_{\mathrm{w}}}\frac{\pi}{2} \\ k_{\mathrm{dn}} = \frac{\sin\left(qn\frac{\alpha}{2}\right)}{N_{turn}\sin\left(n\frac{\alpha}{2}\right)} \end{cases} \quad (14)$$

TABLE I WINDING FACTOR COMPARISON

Symbol	Parameter	without spatial high-order harmonics	with spatial high-order harmonics
N_{m}	*Number of mover slots*	12	
N_{s}	*Number of stator slots*	7	
α	*Slot angle*	30	60
N_{coil}	*Number of coil turns*	42	
k_{pn}	*Pitch factor*	0.97	1
k_{dn}	*Distribution factor*	0.97	1
k_{wn}	*Winding factor*	0.93	1

III. PERFORMANCE EVALUATION

To ensure a fair comparison, the basic design parameters are held constant throughout the design process, with their values detailed in Table II. Other geometric parameters are shown in Fig.6 with their detailed values shown in Table III.

TABLE II BASIC DESIGN PARAMETERS OF THE PROPOSED MACHINE

Symbol	Parameter	unit	Prop. Design
H_{total}	*Total length along Y-axis*	mm	82
L_{m}	*Mover length*	mm	210
δ	*Air-gap length*	mm	1
P_{loss}	*Copper loss*	W	180
v_{m}	*Velocity*	m/s	2

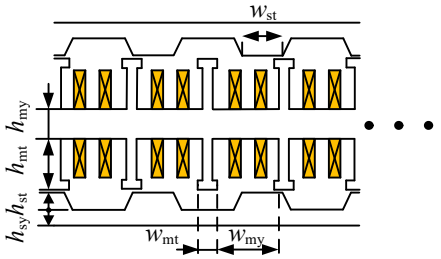

Fig.6. Geometric parameters of VF-VRLM

TABLE III DESIGN PARAMETERS OF THE PROPOSED MACHINE

Symbol	Parameter	unit	Prop. Design
k_{sp}	*Split ratio of mover to stator*		0.7
k_{dc}	*DC component to total loss ratio*		0.5
h_{my}	*Height of mover yoke*	mm	12.5
h_{sy}	*Height of stator yoke*	mm	5
k_{st}	*Ratio of w_{st} to pole pitch*	-	0.35
k_{sm}	*Ratio of w_{st} to w_{mt}*	-	1.2
N_{coil}	*Number of turns in one coil*	-	42

A. Flux distributions

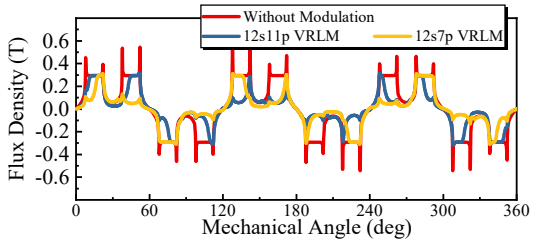

Fig. 7. Air-gap flux densities.

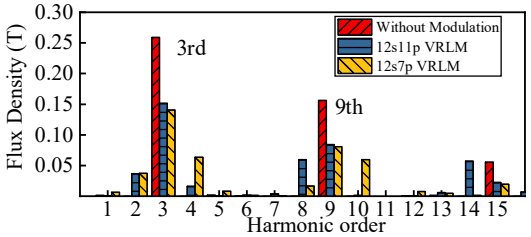

Fig. 8. Air-gap flux densities spectrum.

The simulation result of the zero-sequence current excited air-gap flux density is shown in the Fig.7 with its spectrum shown in the Fig.8 According to the analysis above, the air-

gap flux density contains many harmonics, and the third-order and the ninth-order harmonic of the flux density generated by the magnetomotive force (MMF) of field excitation is abundant in the air-gap. Modulated by the stator teeth of VRLM, 2nd, 8th and 14th order working harmonics are generated in VRLM with 11 poles and 2nd, 4th and 10th order working harmonics are generated in the machine with 7 poles. To obtain higher gear ratio, G_r, 2nd order harmonic is selected as main working harmonic in this paper, and G_r reach 3.5 in the machine with 7 poles and 5.5 in the machine with 11 poles.

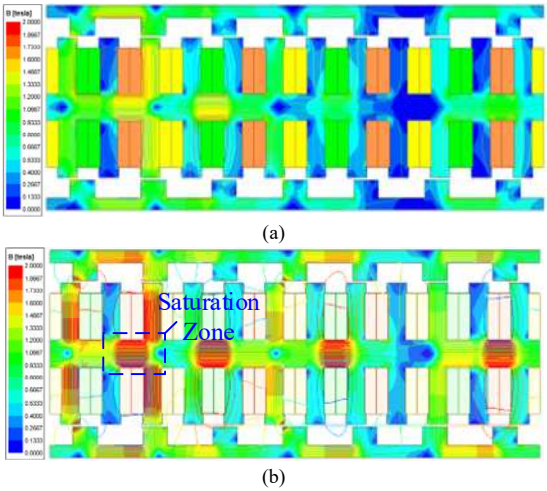

Fig. 9. Flux distributions (a) Rated condition. (b) Overloaded condition.

The flux distributions under rated and overloaded conditions are shown in Fig.9. Due to the lower pole pair number of the working harmonic, the length of magnetic flux is longer than the conventional design with pole pair number of the working harmonic is larger, which is consistent with the analysis. When the copper loss of the winding is twice of the rated condition, the magnetic field distribution undergoes noticeable changes, as depicted in Fig.9 (b). Under these conditions, it can be observed that the motor experiences increased saturation, especially in the mover yoke of DS-VRLM. Therefore, the mover yoke needs to be designed extra wide to avoid saturation issue.

B. *Open-circuit Performance*

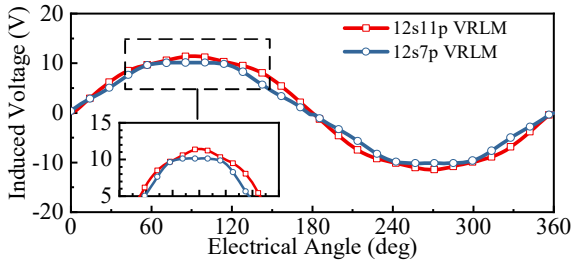

Fig. 10. Induced voltage under open-circuit condition.

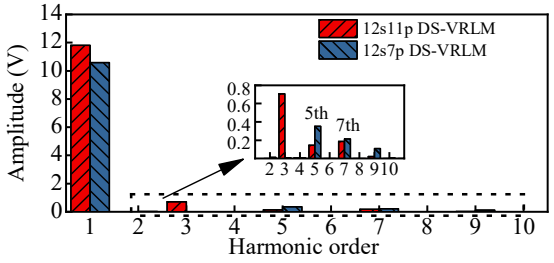

Fig. 11 Induced voltage spectrum.

The open-circuit performances of VRLM with 7 poles and 11 poles under rated condition are illustrated in Fig.10 and Fig. 11. The induced voltage of the machine with 11 poles possesses less harmonics contents at rated condition than that with 7 poles. It should be noticed that the third-order harmonic existing in the induced voltage of the machine with 11 stator poles will not generate extra force ripple when the fundamental sinusoidal current is fed into the machine. Therefore, machine with 11 poles could achieve lower thrust force ripple theoretically.

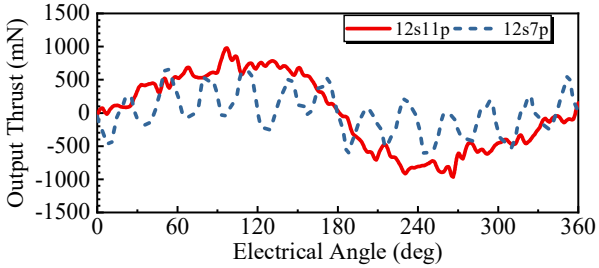

Fig. 12. Detent force of the proposed machine.

The detent forces of the machines with different slot pole combinations are shown in Fig.12. The fundamental harmonic in the detent force is caused by end effect of the machine, and 12th order harmonic also exists in the detent force due to the cogging effect. The peak-to-peak fluctuation of the detent force remains to be relatively low (within 1N).

C. *Thrust Force Performance*

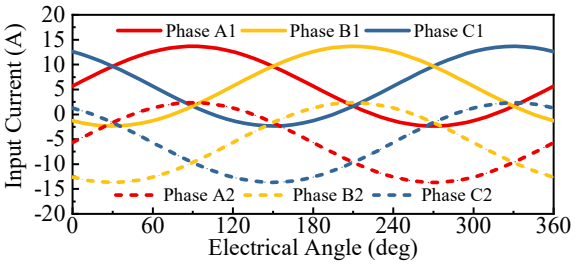

Fig. 13. Input current waveform.

Fig.13 illustrates the rated input current of the six winding terminals, which shows that two windings in the same phase have the same AC current components with the same electrical angle. However, sub-phase A+, B+ and C+ carries a positive DC current under the zero-sequence current control, whereas sub-phase A−, B−, C− is negatively biased with the same zero-sequence DC current.

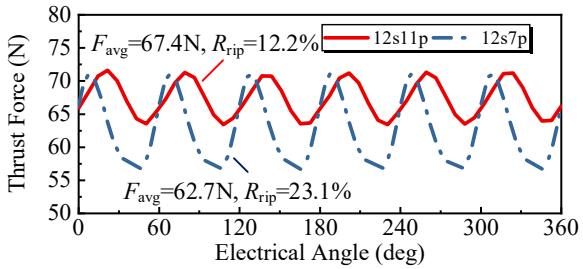

Fig. 14. Output thrust waveform.

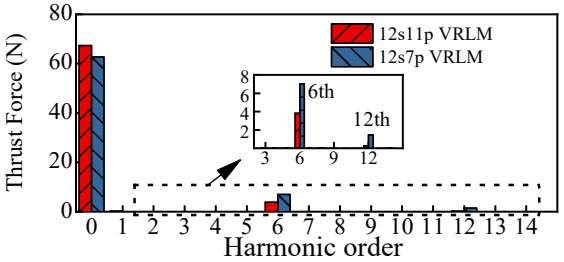

Fig. 15. Output thrust spectrum.

As shown in Fig.14, at rated condition, the proposed machine with 11 poles could achieve 67.4N thrust force and the force ripple is 12.2%, when the sinusoidal current is applied to the proposed machine. For the machine with 7 poles, 62.7N of thrust force could be achieved and the force ripple is much higher, which has reached 23.1%. The spectrum of output torque result is shown in Fig.15. According to the FFT analysis, there are 6th order harmonic and 12th order harmonic existing in the thrust force of the machine with 7 poles, which are mainly caused by the high order harmonics in the induced voltage. And the machine with 11 poles possesses less harmonics in the thrust.

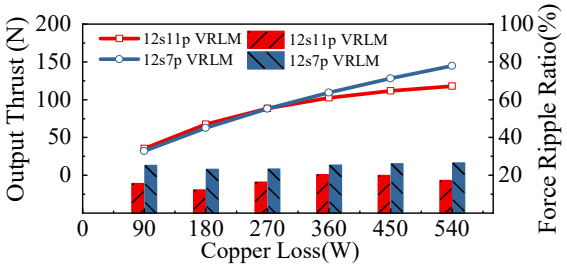

Fig. 16. Average output thrust at different conditions.

As the winding copper loss increases, the output thrust of the motor also rises as shown in Fig.16. Due to the saturation issue of the motor, the rate of increase slows down, when the excitation is doubled to that at rated condition. The proposed machine with 7 poles could achieve higher peak thrust force than that with 11 poles, but results in higher force ripple. With the increase in excitation, the thrust ripple also experiences a slight increase. This behavior underscores the motor's capability to maintain performance stability under varying excitation conditions, making it suitable for applications requiring inconsistent thrust output. To illustrate the superiority of the proposed DL- ITW utilizing working harmonics modulated from spatial higher order harmonics, the performances of proposed machine are compared with conventional variable flux reluctance linear machine, which is summarized in the table.

TABLE IV DESIGN PARAMETERS AND PERFORMANCES COMPARISONS

	VF-RLM [13]	Proposed 12s7p	Proposed 12s11p
L_m, Mover teeth length (mm)		210	
L_{stk}, Stack length (mm)		50	
F_f, Filling factor		0.45	
k_{sp}, Split ratio	0.75	0.70	0.70
k_{dc}, DC to total loss ratio	0.48	0.5	
P_{loss}, copper loss (W)		180	
N_{ac}, Number of AC turns per slot	55	110	110
N_{dc}, Number of DC turns per slot	55	-	-
i_{ac}, AC component amplitude (A)	11.71	8.42	8.42
i_{dc}, DC component current (A)	8.20	5.65	5.65
f_t, Rated thrust force (N)	45.5	62.7	67.4
R_{rip}, Force ripple ratio (%)	16.0	23.1	12.2
D_t, Thrust force density(kN/m^3)	54.2	72.8	78.3
f_{max}, Peak thrust force (N)	111.2	144.7	117.9

IV. CONCLUSION

This paper introduced a novel double layer integrated toroidal winding design for the DS-VRLM, aimed at eliminating extra DC windings and enhancing thrust force density. By utilizing zero-sequence current to excite the winding, the proposed design leverages working harmonics utilizing spatial high-order harmonics, particularly the third-order harmonic in this article which can be utilized as the main working harmonic of the armature winding to optimize the machine's performance. This approach significantly improves the gear ratio of working harmonics and winding factor, as demonstrated by two slot/pole combinations (12s/7p and 12s/11p). The innovative winding configuration, with coils arranged in the same slot but divided into two windings with same or opposite zero-sequence current polarity, allows for flexible regulation of the excitation field. The simulation result shows that the proposed machine can achieve output thrust of 62.7N at rated condition and 144.7N at peak conditions. The comparative results confirm the feasibility and effectiveness of the proposed design, marking a significant advancement in the development of PM-free linear machines with high thrust force density.

ACKNOWLEDGEMENT

This work was supported by the National Natural Science Foundation of China under Project 52077187 and in part by the Research Grant Council, Hong Kong, China, under Project PolyU 152109/20E.

V. REFERENCES

[1] I. Boldea, L. N. Tutelea, W. Xu and M. Pucci, "Linear Electric Machines, Drives, and MAGLEVs: An Overview," in *IEEE Transactions on Industrial Electronics*, vol. 65, no. 9, pp. 7504-7515, Sept. 2018, doi: 10.1109/TIE.2017.2733492.

[2] J. W. Jansen, J. P. C. Smeets, T. T. Overboom, J. M. M. Rovers and E. A. Lomonova, "Overview of Analytical Models for the Design of Linear and Planar Motors," in *IEEE Transactions on Magnetics*, vol. 50, no. 11, pp. 1-7, Nov. 2014, Art no. 8206207, doi: 10.1109/TMAG.2014.2328556.

[3] G. Stumberger, B. Stumberger and D. Dolinar, "Identification of linear synchronous reluctance motor parameters," in *IEEE Transactions on Industry Applications*, vol. 40, no. 5, pp. 1317-1324, Sept.-Oct. 2004, doi: 10.1109/TIA.2004.834118.

[4] J. Du, D. Liang and X. Liu, "Performance Analysis of a Mutually Coupled Linear Switched Reluctance Machine for Direct-Drive Wave Energy Conversions," in IEEE Transactions on Magnetics, vol. 53, no. 9, pp. 1-10, Sept. 2017, Art no. 8108110.

[5] W. Li, K. T. Chau, C. Liu and C. Qiu, "Design and Analysis of a Flux-Controllable Linear Variable Reluctance Machine," in *IEEE Transactions on Applied Superconductivity*, vol. 24, no. 3, pp. 1-4, June 2014, Art no. 5200604, doi: 10.1109/TASC.2013.2284720.

[6] Z. Li and S. Niu, "Overview on Variable Flux Reluctance Linear Machines for Long- Stroke Applications," in *IEEE Transactions on Transportation Electrification*, doi: 10.1109/TTE.2024.3389713.

[7] N. S. Lobo, H. S. Lim and R. Krishnan, "Comparison of Linear Switched Reluctance Machines for Vertical Propulsion Application: Analysis, Design, and Experimental Correlation," in *IEEE Transactions on Industry Applications*, vol. 44, no. 4, pp. 1134-1142, July-aug. 2008, doi: 10.1109/TIA.2008.926294.

[8] T. Jiang, L. Xu, J. Ji and W. Zhao, "Comparative Study of Linear Variable Flux Reluctance Machine with Linear Wound Field Flux Reversal Machine," in *CES Transactions on Electrical Machines and Systems*, vol. 7, no. 1, pp. 73-80, March 2023, doi: 10.30941/CESTEMS.2023.00006.

[9] Y. Shen and Q. Lu, "Investigation of Novel Multi-Tooth Linear Variable Flux Reluctance Machines," in *IEEE Transactions on Magnetics*, vol. 54, no. 11, pp. 1-5, Nov. 2018, Art no. 8107905, doi: 10.1109/TMAG.2018.2839662.

[10] Z. Li, X. Zhao and S. Niu, "Novel High-Order-Harmonic Toroidal Winding Design Approach for Double-Sided Vernier Reluctance Linear Machine," in *IEEE Transactions on Industrial Electronics*, vol. 70, no. 10, pp. 9823-9834, Oct. 2023, doi: 10.1109/TIE.2022.3224133.

[11] Q. Wang, S. Niu, S. L. Ho, W. Fu, and S. Zuo, "Design and analysis of novel magnetic flux-modulated mnemonic machines," *IET electric power applications*, vol. 9, no. 7, pp. 469–477, 2015, doi: 10.1049/iet-epa.2014.0388

[12] F. Ni, S. Niu, Z. Li and X. Zhao, "Novel Slot-Opening-PM Vernier Reluctance Machine with High-Order-Harmonic Winding," in *IEEE Transactions on Magnetics*, vol. 59, no. 11, pp. 1-6, Nov. 2023, Art no. 8103806, doi: 10.1109/TMAG.2023.3296816.

[13] J. Ou, Y. Liu, M. Schiefer, and M. Doppelbauer, "A Novel PM-Free High-Speed Linear Machine with Amorphous Primary Core," *IEEE Transactions on Magnetics*, vol. 53, no. 11, pp. 1-8, 2017, doi: 10.1109/tmag.2017.2701152